Structural, optical and magnetic properties of Gd-doped ZnO thin films for spintronics applications

E. R. SHAABAN[a,*], GH. ABBADY[b], EL SAYED YOUSEF[c,d], GOMAA A. M. ALI[e,f], SAFWAT A. MAHMOUD[g], N. AFIFY[b]

[a]*Physics Department, Faculty of Science, Al-Azhar University, Assiut 71524, Egypt*
[b]*Physics Department, Faculty of Science,* Assiut University, *Assiut,71516, Egypt*
[c]*Research Center for Advanced Materials Science (RCAMS), King Khalid University, Abha 61413, P. O. Box 9004, Saudi Arabia*
[d]*Physics Dep., Faculty of Science, King Khalid University, P. O. Box 9004, Abha, Saudi Arabia*
[e]*Chemistry Department, Faculty of Science, Al-Azhar University, Assiut, 71524, Egypt*
[f]*Faculty of Industrial Sciences & Technology, Universiti Malaysia Pahang, Gambang, 26300 Kuantan, Malaysia*
[g]*Physics Department, Faculty of Science, Northern Border University, Arar 91431, Saudi Arabia*

Different compositions of the bulk sample of $Zn_{1-x}Gd_xO$ (x = 0, 0.02, 0.04, 0.06, 0.08 and 0.1) are fabricated using co-precipitation technique. The current study investigates the structural, optical and magnetic properties of ZnO thin films doped by Gd. The desired films were deposited onto highly-clean glass substrates by electron beam technique. X-ray diffraction revealed the formation of hexagonal wurtzite single phase of ZnO and having intense (002) peak with a peak shift towards lower angle. The crystallite size of the films was found to be decreased with increasing Gd content. The effect of Gd dopant on the optical and magnetic properties of the prepared thin films was investigated. The optical energy gap decreases from 3.27 to 3.11 eV with increasing Gd content. In addition, ferromagnetism initially increases up to optimal Gd concentration at 0.06 after that the ferromagnetism decreases with increasing Gd concentration (at 0.08 and 0.1). The changes in the optical and magnetic properties of the prepared films were discussed based on the structural modification, which, further, enhances upon Gd-doping.

(Received August 31, 2018; accepted April 8, 2019)

Keywords: $Zn_{1-x}Gd_xO$ thin films, Structure Parameters, Optical, Energy gap, Ferromagnetism

1. Introduction

ZnO has interesting properties such as wide band gap (3.37 eV) with large exciton binding energy (60 meV), low dielectric constant, high chemical stability, large electrochemical coupling coefficient, high thermal conductivity and UV protection [1-3]. ZnO films possess high transmittance in the visible and infrared spectral regions and high refractive index, which extend their application range. Recently, diluted magnetic semiconductor (DMS) attracted the attention because of their unique properties such as electronic, magnetic and magneto-optical properties [4, 5]. Their structural, electrical and optical properties can be varied by tunability of lattice parameters, microstructural parameters and energy gaps with respect to the concentration of transition metal (TM) [6, 7]. But, generating reproducible long-range ferromagnetism (FM) in wide bandgap-DMS materials still a major obstacle to the fabrication of spintronic devices operating above room temperature [7, 8]. Some of the experimental studies have shown that the doping of metals with rare earth (RE) such as doping GaN with Gd^{3+} ion can enhance the ferromagnetic property [9]. This motivates the researchers towards RE metal ion doping in metal oxide materials for spintronics applications. In particular, Gd^{3+} has a great interest due to its scintillation and optical devices in the place of other luminescent and large magnetic behavior materials [10-12]. Gd-doped ZnO can produce stronger FM, relative to that obtained from transition metals doped ZnO, this may be due to the possible interaction between localized ^{4}f electrons and host electrons which remains controversial. Ferromagnetism in ZnO doped with rare earth has been attributed to the crystal defect induced [13, 14] Gd doped ZnO have many advantages. It has been reported that Gd ions doped into ZnO enhances hole conductivity because holes in ^{4}f Gd are more active than electrons [15]. In addition, Gd doped ZnO has been found to have a colossal magnetic moment at room temperature [16], which can be used in the fabrication of ZnO based spin electronic devices. Gd doped ZnO nanomaterials are believed to have significant potential in the fields of light-emitting displays, catalysis, drug delivery,and optical storage [17]. The aim of the present work is to study the role of Gd-doping and defects on the structural, optical and magnetic properties of Gd:ZnO thin films for spintronics applications.

2. Experimental

Different compositions of the bulk samples of $Zn_{1-x}Gd_xO$ (x = 0, 0.02, 0.04, 0.06, 0.08, and 0.1) were

fabricated using co-precipitation technique of $Zn(NO_3)_2.6H_2O$ with the appropriate amount of $Gd(NO_3)_3.6H_2O$ to make the required doping percentage dissolved in 50 ml of distilled water. Zinc and Gadolinium nitrates are dissolved in deionized water and then kept stirring for 1 hour. NH_4OH solution was added dropwise till the pH of the solution has reached 9. This mixture was stirred for 2 hours at room temperature and, consequently, filtered. The precipitate was dried at 80 ^oC for 4 hours.

The thermogravimetric analysis (TGA) (Shimadzu 50) of the precursor was performed. According to TGA analysis, the calcination temperature was chosen to be 450 ^oC for 2 hours in order to get a polycrystalline powder. Different $Zn_{1-x}Gd_xO$ thin films with the same thickness were evaporated in terms of electron beam gun technique with a vacuum of about 10^{-6} Pa. The evaporation rate, as well as film thickness, was controlled using a quartz crystal FTM6 monitor. The deposition rate was maintained constant at about 2 nm/s during the sample preparation. Such a low deposition rate can produce a film with a composition very close to that of the bulk starting material.

The structure of the powder and thin films of $Zn_{1-x}Gd_xO$ were measured using X-ray diffraction (XRD, Shimadzu X-ray diffractometry 6000, Japan) with Cu-K_α radiation having λ = 0.15418 nm. The intensity data was collected by step scan modes of a 2θ range between 5^o and 70^o with a step size of 0.02^o and step time of 0.6 s. The pure silicon (≈ Si 99.9999 %) is used as an internal standard. The composition of the synthesized polycrystalline particles is quantified by energy-dispersive analysis of X-ray (EDAX) using energy-dispersive X-ray (EDX) spectrometer. The optical transmittance of the deposited films is measured using a UV-VIS-NIR JASCO V-670 double-beam spectrophotometer. The transmittance spectra in the wavelength range of 240-1100 nm were collected at normal incidence without a substrate in the reference beam. The magnetic properties of the prepared films were studied using the vibrating sample magnetometer model (VSM-9600M-1, USA). The measurements were conducted at room temperature in a maximum applied field of 15 kOe.

3. Results and discussion

3.1. Structural properties

TGA is one of the major thermal analysis technique which is used to study the thermal behavior of precursor materials. TGA was carried out at the temperature range extended from room temperature to 700 °C as shown in Fig. 1. From this figure, a weight loss about 17% was associated with the three following phases, the first weight loss of about 9% occurred until 361°C is attributed to the removal of water which is adsorbed on the surface of the material. The second weight loss of about 7% occurred between 361°C to 450 °C may be attributed to the complete crystallization of zinc oxide from the amorphous nature. The third weight loss about 2% is due to the oxidation of residue compounds.

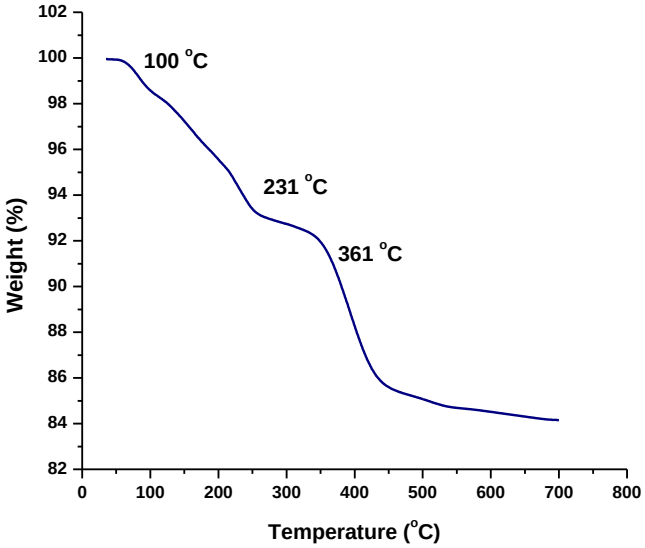

Fig. 1. Thermogravimetric analysis of the precursor

EDAX can be used in order to identify peaks that correspond to the elements present in the film. The highest peak in the spectrum is the more concentrated the element is in the spectrum. EDAX data is shown in Fig. 2 and depicts the presence of Zn and Gd atoms in the prepared $Zn_{0.94}Gd_{0.06}O$ film. The absence of other elements in the spectra confirms the purity of the film sample.

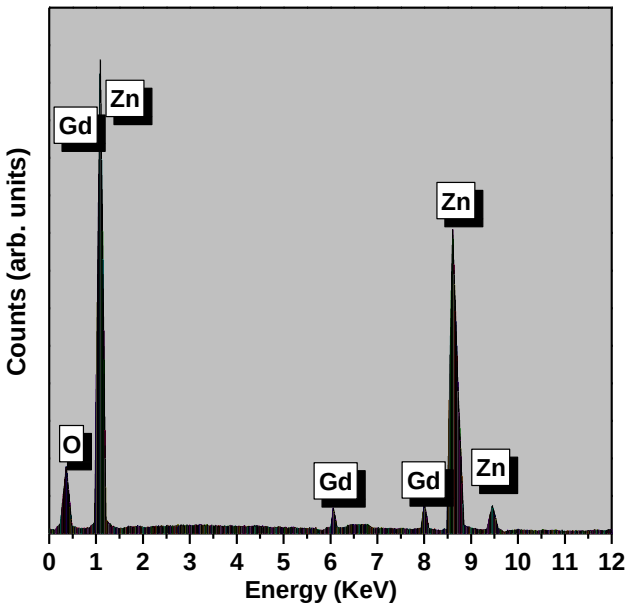

Fig. 2. Energy-dispersive analysis of X-ray spectra $Zn_{0.94}Gd_{0.06}O$ thin film

The X-ray diffraction patterns of the as-deposited ZnO and Gd-doped ZnO in $Zn_{1-x}Gd_xO$ thin films are shown in Fig. 3. The patterns of $Zn_{1-x}Gd_xO$ thin films were compared with standard JCPDS data. All of the diffraction peaks are perfectly indexed to the hexagonal wurtzite ZnO

structure (JCPDS 01-1136), revealing that the doping of Gd does not change the crystal structure of ZnO. The absence of the Gd traces or any other impurity phase of diffraction peaks in the XRD pattern confirms the formation of the $Zn_{1-x}Gd_xO$ solid. Moreover, Fig. 3 shows that the intensity of the preferential orientation (002) plane peaks decreases with increasing Gd concentration and shifted towards lower values of the diffraction angle (see Fig. 4). The shift in the peak position is due to higher ionic radii of Gd^{2+} ions (r = 0.094 nm) relative to the ionic radii of Zn^{2+} ions (r = 0.074 nm). In addition, the full width at half maximum (FWHM) increases with increasing Gd content as shown in Fig. 5. This behavior implies a decrease in crystallite size and thus the crystalline quality of the thin films. The crystallite size (*D*) can be calculated by using Scherrer formula [18, 19]:

$$D = \frac{0.9\lambda}{\beta \cos\theta} \tag{1}$$

where λ is the incident wavelength and β is the structural broadening that equal the difference in integral X-ray peak profile width between the sample and a standard (silicon) and it is given by $\beta = \sqrt{\beta_{obs}^2 - \beta_{std}^2}$.

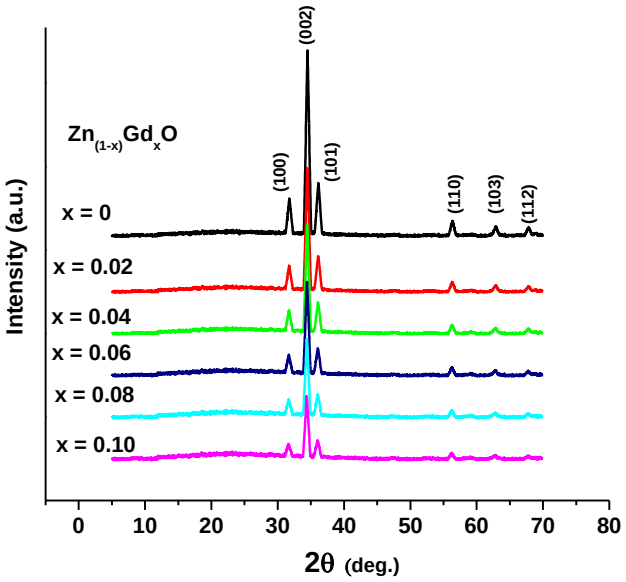

Fig. 3. X-ray diffraction patterns of polycrystalline $Zn_{1-x}Gd_xO$ thin films

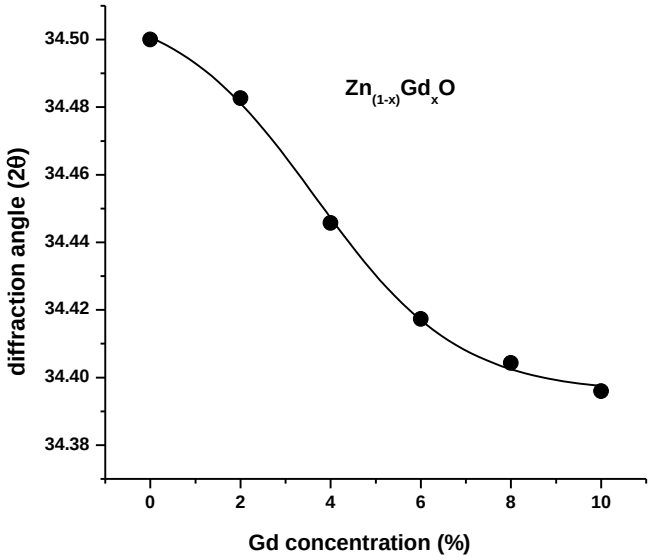

Fig. 4. Diffraction angles as a function of Gd concentration for $Zn_{1-x}Gd_xO$ thin films

Fig. 5 shows that the *D* values decrease with increasing the Gd content. This decrease in crystallite size is due to the creation of oxygen vacancies with Gd ions, that reduce lattice parameters and result in strong tensile stress [20]. Also, the incorporation of Gd dopant inhibits the agglomeration phenomenon among ZnO particles, and hence, results in a decrease in average crystallite size [21].

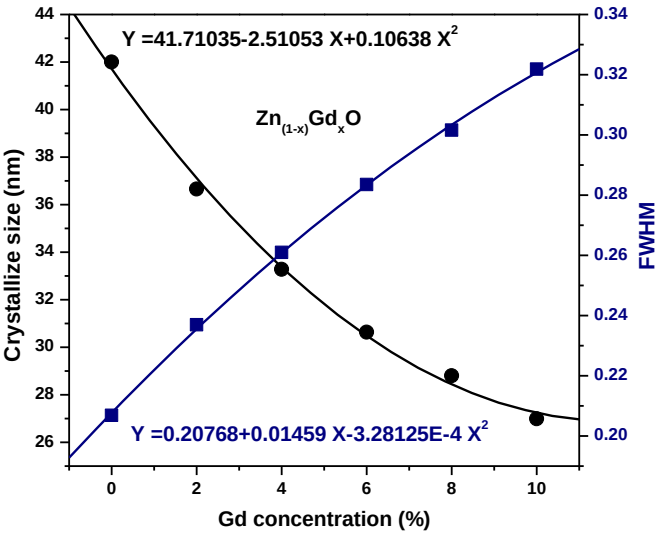

Fig. 5. Crystalline size and FWHM as a function of Gd concentration of $Zn_{1-x}Gd_xO$ thin films

3.2. Optical properties

Optical properties of the as-deposited ZnO and Gd-doped ZnO in $Zn_{1-x}Gd_xO$ thin films were investigated using UV-Vis transmission spectra (Fig. 6). All transmissions of the films appear with fringes without shrinkage in amplitude particularly in medium absorption region, which indicates the homogenous structure of deposited films. Furthermore, the absorption edge of the deposited films shows a red shift with increasing Gd at expense of Zn in $Zn_{1-x}Gd_xO$ thin films as shown in the inset of Fig. 6. This trend indicates that the Gd affects the transmission spectra thus the energy gap of the deposited films.

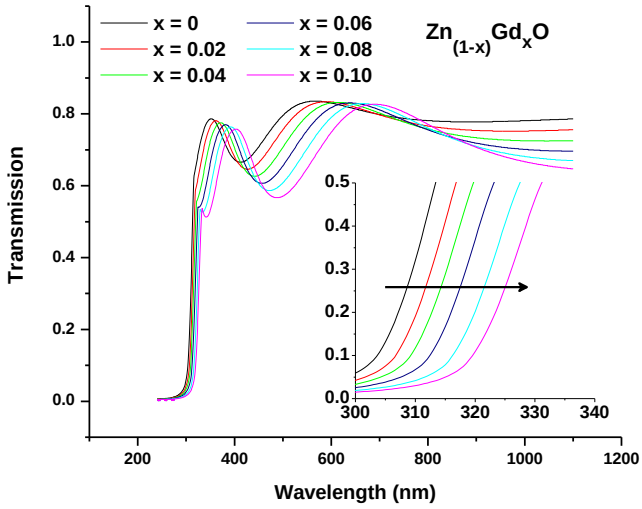

Fig. 6. A typical optical transmission-reflection spectra of $Zn_{1-x}Gd_xO$ thin films

According to the envelope method of transmission spectrum, the value of refractive index at a certain wavelength can be calculated using the following relationship [22-24]:

$$n = \left[N_1 + (N_1^2 - s^2)^{\frac{1}{2}} \right]^{\frac{1}{2}} \quad (2)$$

where

$$N_1 = 2s\frac{T_M - T_m}{T_M T_m} + \frac{s^2 + 1}{2} \quad (3)$$

where T_M and T_m are the transmittance maximum and the corresponding minimum at a certain wavelength as shown in Fig. 7 a and b.

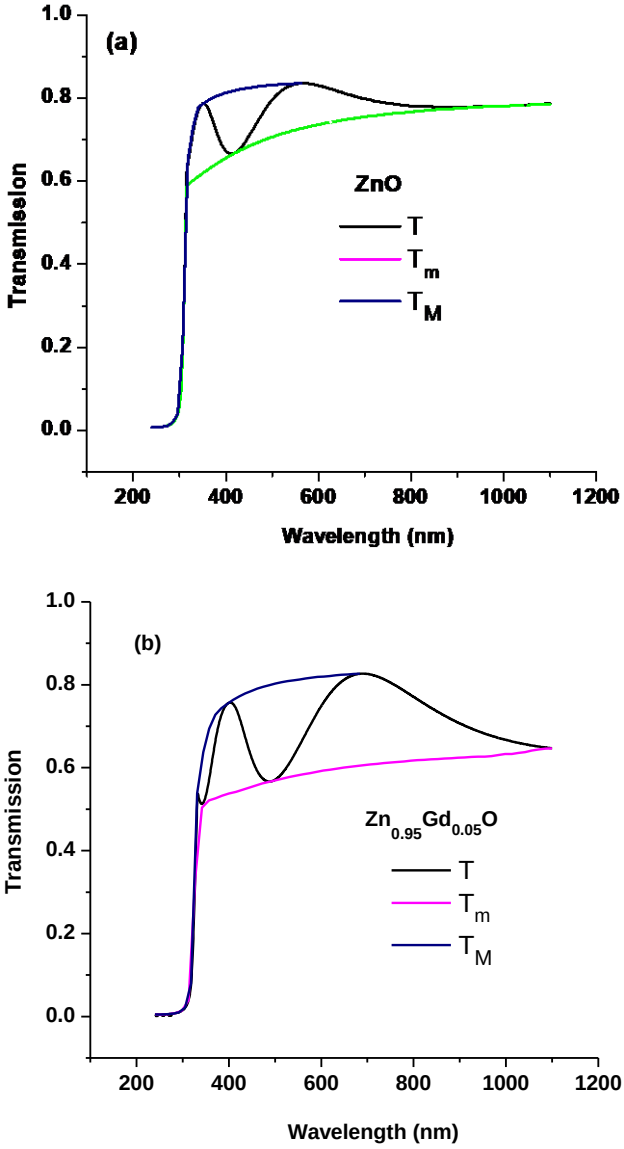

Fig. 7. A typical optical transmission-reflection spectra of (a) ZnO and (b) $Zn_{0.95}Gd_{0.05}O$

The value of the refractive index of the substrate can be obtained from the transmittance spectrum of the substrate (T_s) using the well-known equation [24]:

$$s = \frac{1}{T_s} + \left(\frac{1}{T_s} - 1\right)^{\frac{1}{2}} \quad (4)$$

In terms of the calculated refractive indices n_1 and n_2 at two adjacent maxima (or minima) at λ_1 and λ_2, respectively, the film thickness is given by the relationship:

$$d = \frac{\lambda_1 \lambda_2}{2(\lambda_1 n_{e2} - \lambda_2 n_{e1})} \quad (5)$$

The values of the film thickness of as-deposited and annealed $Zn_{1-x}Gd_xO$ thin films was about 150 ± 2% nm. The refractive index of all these films displays normal dispersion i.e. decrease with increasing wavelength (see Fig. 8) that follows Sellmeier equation [25]:

$$n^2 = 1 + \frac{A_o \lambda^2}{\lambda^2 - \lambda_o^2} \tag{6}$$

Rearrange this equation gives:

$$\frac{1}{n^2 - 1} = -\frac{A}{\lambda^2} + B \tag{7}$$

where $A = \lambda_0^2 / A_0$ and $B = 1/A_0$

By plotting the relationship between $1/(n^2\text{-}1)$ and $1/\lambda^2$ the slope, A and intercept, B can be determined thus λ_o and A_o as well. The Sellmeier coefficient are listed in Table 1, can be used for both interpolation and extrapolation over the whole wavelength range as shown in Fig. 8.

Table 1. The Sellmeier coefficient and energy gap of $Zn_{1-x}Gd_xO$ films

Gd content (%)	Sellmeier coefficients				E_o (eV)
	A	B	A_o	λ_o (nm)	
0	5.152	0.455	2.200	336.7	3.27
2	4.194	0.392	2.554	327.3	3.22
4	3.412	0.34	2.943	316.9	3.18
6	2.727	0.301	3.327	301.2	3.15
8	2.234	0.261	3.827	292.4	3.12
10	1.791	0.231	4.320	278.2	3.10

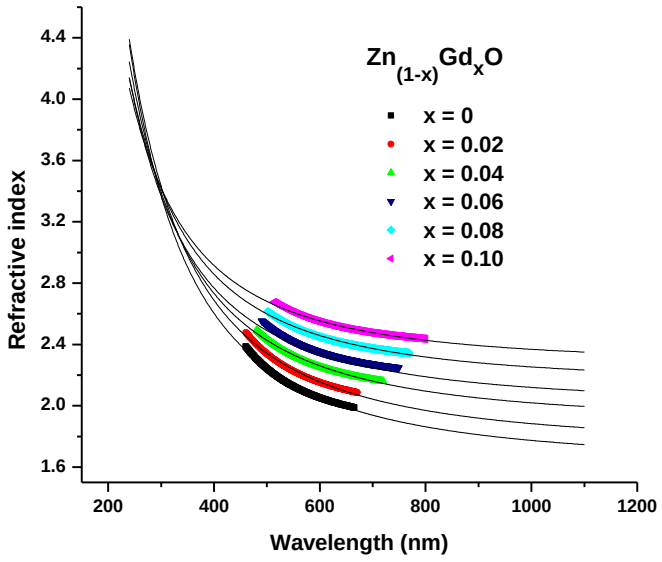

Fig. 8. Dispersion of refractive index of polycrystalline $Zn_{1-x}Gd_xO$ thin films obtained from transmission spectra

The absorption coefficient (α) of $Zn_{1-x}Gd_xO$ can be calculated in the strong absorption region of transmission spectra using the following relationship:

$$T = \frac{A}{B} e^{-\alpha d} \tag{8}$$

where $A = 16n^2 s$ and $B = (n+1)^3/(n+s^2)$

In the strong absorption region, the interference fringes disappear and the two curves T_{max} and T_{min} converge to a single curve. A and B depend on the refractive index (*n*) of the thin film and refractive index of the substrate (s). By knowing the value of thickness (*d*), the values of n can be extrapolated in the strong absorption region in terms of Sellmeier Eq., thus the absorption coefficient (α) can be calculated using the following expression [26-28]:

$$\alpha = \frac{1}{d} \ln\left(\frac{A}{BT}\right) \tag{9}$$

Fig. 9 shows the variation of α(hν) as a function of hν for $Zn_{1-x}Gd_xO$ films. Absorption of photons causes a transition of the electrons from valence band to conduction band. The absorption ability is measured by its absorption coefficient (α) which is a function of frequency [29-31]. For allowed direct band-to-band transitions, the α(hν) is described as:

$$\alpha(h\upsilon) = \frac{\beta(h\upsilon - E_g^{opt})^m}{h\upsilon} \tag{10}$$

where β is a characteristic parameter (independent of photon energy) for respective transitions and *m* is a number that characterizes the transition process. m = 2 for most amorphous semiconductors (indirect transition) and m =1/2 for most crystalline semiconductor (direct transition) [32-35]. According to polycrystalline nature of the XRD films, as shown in Fig. 3, thus the allowed direct optical band gaps of $Zn_{1-x}Gd_xO$ are evaluated from $(\alpha h\nu)^2$ against hν plot and extrapolated to intersect the energy axis at $(\alpha h\nu)^2 = 0$ gives the direct E_g^{opt} (see Fig. 10).

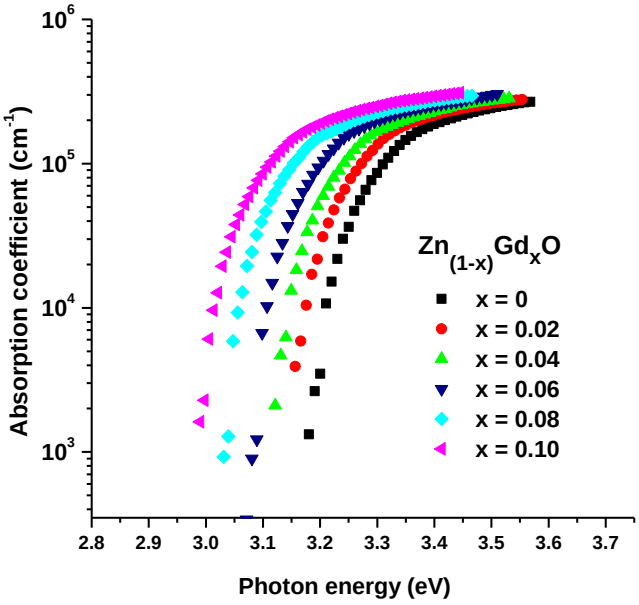

Fig. 9. The absorption coefficient versus photon energy for the polycrystalline $Zn_{1-x}Gd_xO$ thin films

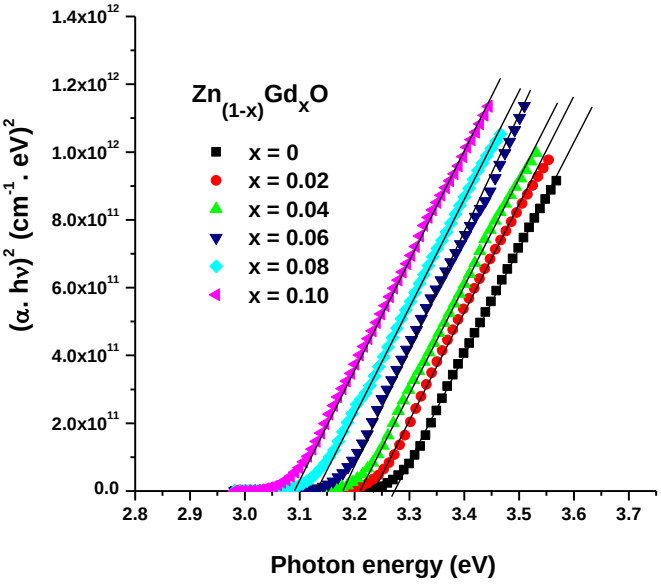

Fig. 10. The dependence of $(\alpha h\nu)^2$ on photon energy for the different compositions of $Zn_{1-x}Gd_xO$ thin films

The variation of direct E_g^{opt} as a function of Gd content is shown in Fig. 11. The values of direct E_g^{opt} are found to decrease with increasing Gd content (see Table 1). This indicates that the doping ions introduce new electronic levels (subbands) inside the ZnO band-gap. These new electronic levels were merged with the conduction band forming continuous band leading to the reduction of the band gap. In addition, the red shift in band gap may be related to the presence of defects such as oxygen vacancies and interstitial oxygen, which certainly are inherent to the synthesis process [36, 37].

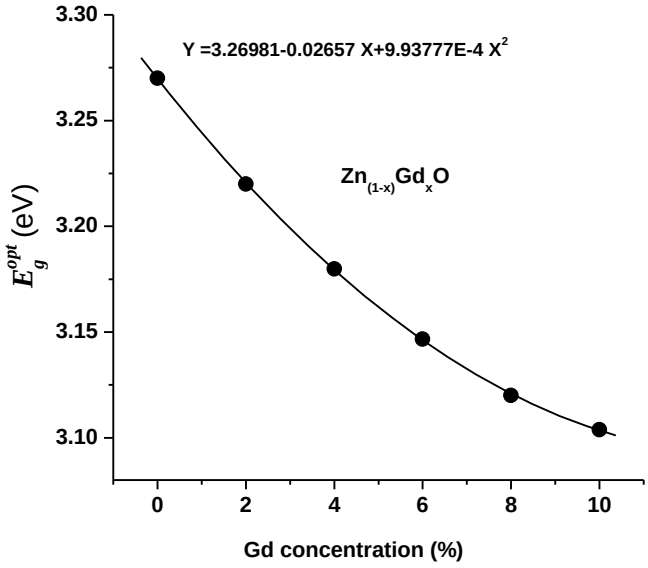

Fig. 11. Variation in optical energy gap as a function of Gd content

The decrease in E_g^{opt} for direct transition may be attributed to the decrease in the crystallite size because the crystal defects can be formed which produce localized states that change the effective Fermi level due to an increase in carrier concentration [38, 39].

3.3. Magnetic properties

The magnetization hysteresis loops (M-H curve) of Gd-doped ZnO films at room temperature are shown in Fig. 12, where the contributions of the FM signals of the films were deducted. The undoped ZnO films showed diamagnetism. Further increasing Gd dopant concentration, ferromagnetism initially increases up to optimal Gd concentration at 6% after that the ferromagnetism decreases with increasing Gd concentration (at 8 and 10%). The saturation magnetization as a function of Gd content in $Zn_{(1-x)}Gd_xO$ is shown in Fig. 13. The calculated saturation magnetism is 0.081, 0.124 and 0.174 emu/g for 2, 4 and 6%, respectively, i.e. increases with increasing Gd content. But at Gd concentration 8 and 10%, the saturation magnetism decreases (0.146 and.0.106 emu/g, respectively). Firstly, the increase in saturation magnetization can be attributed to oxygen vacancies, which generates long range ferromagnetism as the doping of Gd ions, in turn; increase the oxygen [40]. Secondly, the decrease in saturation magnetization can be explained due to antiferromagnetic alignment caused by the increased number of Gd atoms occupying adjacent cation positions. A similar effect was observed in Co-doped ZnO [41] and Er-doped ZnO [42] systems.

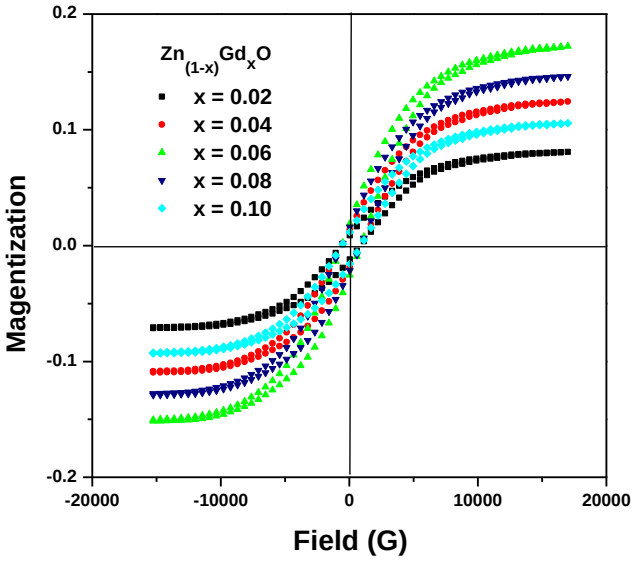

Fig. 12. Magnetization hysteresis loops for the different compositions of $Zn_{1-x}Gd_xO$ thin films

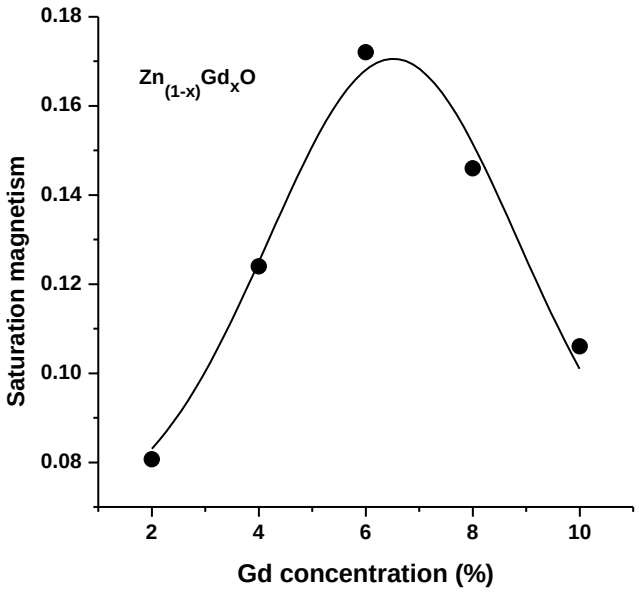

Fig. 13. Saturation magnetization as a function of Gd content

4. Conclusions

Co-precipitation method was used to prepare different compositions of the bulk sample of $Zn_{1-x}Gd_xO$ (x = 0, 0.02, 0.04, 0.06, 0.08 and 0.1) and then deposited as thin films onto highly-clean glass substrates by electron beam technique. The structural, optical and magnetic properties of ZnO thin films doped by Gd were investigated in details. The films show formation of hexagonal wurtzite single phase of ZnO and having intense (002) peak with a peak shift towards lower angle. The crystallite size of the films was found to be decreased from 42 nm to 10 nm with increasing Gd content from 0 to 0.1. The optical energy gap decreases from 3.27 to 3.11 eV with increasing Gd content. In addition, ferromagnetism initially increases up to optimal Gd concentration at 0.06 after that the ferromagnetism decreases with increasing Gd concentration (at 0.08 and 0.1). The changes in the optical and magnetic properties of the prepared films were discussed based on the structural modification, which, further, enhances upon Gd-doping.

Acknowledgment

The authors thank Al-Azhar University and Assiut University for providing the facilities during samples preparation and testing. In addition, the authors thank the the Deanship of King Khalid University, the Ministry of Education, and Kingdom of Saudi Arabia for financing this research through a grant (RCAMS/KKU/001-18) under research center for advanced material science.

References

[1] M. Bouloudenine, N. Viart, S. Colis, J. D. Kortus, Appl. Phys. Lett. **87**, 052501 (2005).
[2] A. S. Risbud, N. A. Spaldin, Z. Q. Chen, S. S. Stemmer, Phys. Rev. B **68**, 205202 (2003).
[3] S. Thota, T. Dutta, J. Kumar, J. Phys.: Condens. Matter. **18**, 2473 (2006).
[4] S. J. Pearton, C. R. Abernathy, M. E. Overberg, G. T. Thaler, D. P. Norton, J. Appl. Phys. **93**, 1 (2003).
[5] X. Wang, J. Xu, B. Zhang, H. Yu, J. Wang, X. Zhang, J. Yu, Q. Li, Adv. Mater. **18** (2006) 2476.
[6] G. Vijayaprasath, R. Murugan, T. Mahalingam, Y. Hayakawa, G. Ravi, Ceram. Int. **41**, 10607 (2015).
[7] G. A. Prinz, Science **282**, 1660 (1998).
[8] S. Chambers, Nat. Mater. **9,** 956 (2010).
[8] G. Vijayaprasath, R. Murugan, T. Mahalingam, Y. Hayakawa, G. Ravi, J. Alloys Comp. **649**, 275 (2015).
[9] S. Dhar, O. Brandt, M. Ramsteiner, V. F. Sapega, K. H. Ploog, Phys. Rev. Lett. **94**, 037205 (2005).
[10] J. S. Bae, J. H. Jeong, S. S. Yi, J. C. Park, Appl. Phys. Lett. **82**, 3629 (2003).
[11] C. D. Pemmaraju, R. Hanafin, T. Archer, H. B. Braun, S. Sanvito, Phys. Rev. B **78**, 054428 (2008).
[12] H. Gu, Y. Jiang, Y. Xu, M. Yan, Appl. Phys. Lett. **98**, 012502 (2011).
[13] X.-L. Li, J.-F. Guo, Z.-Y. Quan, X.-H. Xu, G. A. Gehring, IEEE Trans. Magn. **46**, 1382 (2010).
[14] C. J. Cong, L. Liao, Q. Y Liu, J. C. Li, K. L. Zhang, Nanotechnology **17**, 1520 (2006).
[15] L. Liu, P. Y. Yu, Z. Ma, S. S. Mao, Physical Review Letters **100**, 127203 (2008).
[16] A. Khodorov, A. G. Rolo, E. K. Hlil, J. Ayres de Campos, O. Karzazi, S. Levichev, M. R. Correia, A. Chahboun, M. J. M. Gomes, Eur. Phys. J. Appl. Phys. **57**, 10301 (2012).
[17] J. Zhong, S. Muthukumar, Y. Chen, Y. Lu, H. M. Ng, W. Jiang et al., Applied Physics Letters **83**, 3401 (2003).

[18] A. L. Patterson, Phys. Rev. **56**, 978 (1939).
[19] O. A. Fouad, S. A. Makhlouf, G. A. M. Ali, A. Y. El-Sayed, Mater. Chem. Phys. **128,** 70 (2011).
[20] A. A. Dakhel, M. El-Hilo, J. Appl. Phys. **107**, 123905 (2010).
[21] A. Khataee, R. D. C. Soltani, A. Karimi, S. W. Joo, Ultrason. Sonochem. **23**, 219 (2015).
[22] E. R. Shaaban, A. Almohammedi, E. S. Yousef, G. A. M. Ali, K. F. Chong, A. Adel, A. Ashour, Optik **164**, 527 (2018).
[23] R. Swanepoel, J. Phys. E: Sci. Instrum. **16**, 121 (1983).
[24] E. R. Shaaban, I. S. Yahia, E. G. El-Metwally, Acta Phys. Pol. A **121**, 628 (2012).
[25] T. Bellunato, M. Calvi, C. Matteuzzi, M. Musy, D. L. Perego, B. Storaci, Europ. Phys. J. **52**, 759 (2007).
[26] F. A. Jenkins, H. E. White, J. Phys. E: Sci. Instrum. **16**, 1214 (1983).
[27] Y. Jin, B. Song, Z. Jia, Y. Zhang, C. Lin, X. Wang, S. Dai, Opt. Express **25**(1), 440 (2017).
[28] E. Marquez, J. B. Ramirez-Malo, P. Villares, R. Jimenez-Garay, R. Swanepoel, Thin Solid Films **234**, 83 (1995).
[29] Y. E. Lee, Y. J. Kim, H. J. Kim, J. Mater. Res. **13**, 1260 (1998).
[30] H. Tabet-Derraz, N. Benramdane, D. Nacer, A. Bouzidi, M. Medles, Sol. Energy Mater. Solar Cells. **73**, 248 (2002).
[31] L. F. Dong, Z. Cui, Z. K. Zhang, Nanostru. Mater. **8**, 815 (1997).
[32] E. R. Shaaban, H. A. Elshaikh, M. M. Soraya, Optoelectron. Adv Mat. **9**, 587 (2015).
[33] E. A. Davis, N. F. Mott, Philos. Mag. **22**, 903 (1970).
[34] E. R. Shaaban, Philos. Mag. **88**, 781 (2008).
[35] E. R. Shaaban, M. Abdel-Rahman, E. Yousef, M. T. Dessouky, Thin Solid Films **515**, 3810 (2007).
[36] E. R. Shaaban, Appl. Phys. A **115**, 919 (2014).
[37] E. R. Shaaban, J. Alloys Compds. **563**, 274 (2013).
[38] G. L. Kabongo, G. H. Mhlongo, T. Malwela, B. M. Mothudi, K. T. Hillie, M. S. Dhlamini, J. Alloys Compds. **591**, 156 (2014).
[39] K. Kaur, G. S. Lotey, N. K. Verma, J. Mater. Sci.: Mater. Electron. **25**, 2605 (2014).
[40] S. Kumar, P. D. Sahare, Mater. Res. Bull. **51**, 217 (2014).
[41] M. Venkatesan, C. B. Fitzgerald, J. G. Lunney, J. M. D. Coey, Phys. Rev. Lett. **93**, 177206 (2004).
[42] J. Qi, Y. Yang, L. Zhang, J. Chi, D. Gao, D. Xue, Scr. Mater. **60**, 289 (2009).

*Corresponding author: esam_ramadan2008@yahoo.com